doi:10.14311/ppt.2023.3.141
Plasma Physics and Technology **10**(3):141–145, 2023

TWO-DIMENSIONAL AXISYMMETRIC MODELING OF THE MAGNETIC FIELD FOR HIGH-VOLTAGE GAS CIRCUIT BREAKERS

B. Galletti[a,*], M. Schwinne[a], M. Buffoni[a], P. U. Cristini[b]

[a] *Hitachi Energy Research, 5401 Baden-Dättwil, Switzerland*

[b] *Hitachi Energy Ltd., 8050 Zurich, Switzerland*

[*] bernardo.galletti@hitachienergy.com

Abstract. High fidelity numerical analyses of high-voltage gas circuit breakers have been conducted at Hitachi Energy Research with an in-house CFD-based arc simulation tool. The tool extends the capability of a commercial flow solver (ANSYS Fluent) to represent physical phenomena at play in a high voltage circuit breaker during a breaking operation, such as magnetostatics, polymeric and metal evaporation, and arc-network interaction. This work describes the implementation of the Biot-Savart law for computing the magnetic field generated by an electric arc under the magnetostatic approximation and in two–dimensional axisymmetric conditions. The implementation is compared to the reference one based on the magnetic vector potential formulation of the Ampère's law in the Coulomb gauge. The limitations of the two formulations are discussed and their numerical accuracy compared.

Keywords: high-voltage circuit breaker, 2D axisymmetric arc simulation, vector potential, Biot-Savart.

1. Introduction

The research and development of high-voltage circuit breakers (HVCBs) rely on experimental and numerical investigations. Experiments are quite expensive and provide only a limited amount of information, typically in integral form and localized in single points. A deeper insight into interruption phenomena can be obtained with the help of computational fluid dynamics (CFD). The arc simulation tool in use at Hitachi Energy Research is based on a commercial CFD software (ANSYS Fluent), whose capabilities are extended by a library of user-defined functions to include magnetostatics, ablation, erosion, and arc-network coupling. This work focuses on the physical and numerical aspects involved in the modeling of the self-induced magnetic field in HVCBs with the magnetostatic approximation. Several authors developed numerical methods to solve this problem. A comprehensive review of these attempts is available in [1].

Given that most of the constitutive elements of HVCBs possess rotational symmetry, these devices are often simulated under the two–dimensional axisymmetric (2D–axi) approximation, which yields indeed accurate results in many applications. In this article, a simple formulation is presented for computing the magnetic fields generated by axisymmetric current distributions. It is based on the Biot-Savart (BS) law and is suitable for the implementation in ANSYS Fluent. The results of this method are compared to those obtained with the numerical integration of the Ampère's circuital law expressed in terms of magnetic vector potential (MVP). Both numerical methods are validated by reproducing the pressure measured in a experiment in which an axisymmetric electric arc was established. The physical model of the arc is detailed in Section 2 with a special focus on the magnetostatic modeling. The numerical methods for solving the magnetostatic problem are presented in Section 3 along with the comparison between numerical and experimental results.

2. The physical model

The physical model characterizing the transient dynamics of the electric arc in a HVCB is expressed by the following governing equations:

$$\partial_t \rho + \nabla\cdot(\rho \boldsymbol{U}) = S_{\mathrm{m,tot}} \tag{1}$$

$$\partial_t(\rho \boldsymbol{U}) + \nabla\cdot(\rho \boldsymbol{U}\otimes\boldsymbol{U}) = -\nabla p + \nabla\cdot\boldsymbol{\tau} + \boldsymbol{j}\times\boldsymbol{B} \tag{2}$$

$$\partial_t(\rho e^o) + \nabla\cdot(\rho \boldsymbol{U} h^o) = \nabla\cdot(\boldsymbol{\tau}\cdot\boldsymbol{U} - \boldsymbol{q}) + \boldsymbol{E}\cdot\boldsymbol{j} + S_{\mathrm{e,tot}} \tag{3}$$

$$\partial_t(\rho Y_i) + \nabla\cdot(\rho \boldsymbol{U} Y_i) = -\nabla\cdot\boldsymbol{\mathcal{F}}_i + S_{\mathrm{m},i} \tag{4}$$

$$\boldsymbol{s}\cdot\nabla I_\lambda = a_\lambda(I_{b\lambda} - I_\lambda) \tag{5}$$

$$\nabla\cdot\boldsymbol{j} = 0 \tag{6}$$

$$\nabla\times\boldsymbol{B} = \mu_0\boldsymbol{j} \tag{7}$$

along with the constitutive relationships for the electromagnetic and gas models. The symbols in the above equations have the following meaning: ρ mass density, $\boldsymbol{U}$ velocity vector, p pressure, $\boldsymbol{\tau}$ stress tensor, e^o stagnation internal energy per unit mass, $h^o = e^o + p/\rho$ stagnation enthalpy per unit mass, $\boldsymbol{q} = -\nabla\cdot(k\nabla T) + \boldsymbol{q}_{\mathrm{rad}}$ total heat flux, k thermal conductivity, T temperature, $\boldsymbol{q}_{\mathrm{rad}}$ radiative heat flux, $\boldsymbol{j}$ current density, $\boldsymbol{E}$ electric field, $\boldsymbol{B}$ magnetic field, $S_{\mathrm{m,tot}}$ total mass source due to evaporation, and $S_{\mathrm{e,tot}}$ total energy source due to evaporation.

The relationships (1), (2), and (3) represent the compressible Reynolds-averaged Navier-Stokes equations (RANS). The flow quantities in these equations are averages from which the turbulent fluctuations have been filtered out. The extra variables introduced

by the averaging of the equations require other equations to be included in order to achieve the closure of the system. These additional equations define the turbulence model and are not reported in the system of equations (1)–(7). Turbulence plays an important role in defining the arc behavior and the way it is modeled has a noticeable influence on the accuracy of simulations conducted for HVCBs. Our CFD-based arc simulation tool implements the $k\omega$-SST turbulence model with Kato-Launder correction, as it showed good accuracy in both the ablation controlled and axially blown stages of the arcing process, for a wide range of in-house validation studies.

The radiative energy emitted by the arc induces evaporation from the surfaces of the nozzles that surround the arcing contacts. Such nozzles are typically made of polytetrafluoroethylene (PTFE) and their ablation is described by the simple model provided in [2]. The other main phase transition taking place in HVCBs concerns the erosion of the arcing contacts, which is modeled by an empirical law that links the metal evaporation to the amount of current flowing through the contacts [3].

The gas inside a HVCB is treated with a multi-species one-fluid model under chemical equilibrium (CE) and local thermodynamic equilibrium (LTE) and its thermodynamic and transport properties have been pre-computed with a Cantera-based tool [4]. The same tool was used in conjunction with the databases [5, 6] to build the absorption spectrum data necessary for the integration of the radiative transfer equation discussed below.

Equation (4) expresses the mass conservation for the i–th species, where Y_i is its mass fraction, $\boldsymbol{\mathcal{F}}_i$ its diffusion flux due to concentration and temperature gradients, and $S_{\mathrm{m},i}$ is the source term expressing the rate of creation the i–th species by evaporation.

The quasi-steady radiative transfer equation (RTE) (5) allows to compute the spectral radiative intensity I_λ for the wavelength λ and in the direction of the unit vector $\boldsymbol{s}$ through a non-scattering medium with absorption coefficient a_λ. The term $I_{b\lambda}$ indicates the spectral radiative intensity for a blackbody. The radiative heat flux that appears on the right-hand side of (3) reads $\boldsymbol{q}_{\mathrm{rad}} = \int_0^\infty \int_{4\pi} I_\lambda \, \boldsymbol{s} \, \mathrm{d}\Omega \, \mathrm{d}\lambda$. The RTE is solved according to the spectral integration method reported in [7].

Regarding the electromagnetic aspects of plasma arcs in HVCBs, we can reasonably assume that both space charge neutrality and magnetostatic approximations apply. Equations (6) and (7) represent the charge continuity equation and the Ampère's law in the context of said approximations. In the Ampère's law, $\mu_0 = 4\pi \cdot 10^{-7}\,\mathrm{H/m}$ is the magnetic permeability of vacuum, while for the relative permeability the approximation $\mu_r \simeq 1$ was made given the absence of magnetic materials in HVCBs. The magnetostatic equations are coupled with the RANS equation through the Lorentz force per unit volume $\boldsymbol{j} \times \boldsymbol{B}$ and the ohmic power per unit volume $\boldsymbol{E} \cdot \boldsymbol{j}$. The coupling is bidirectional as the RANS equations feed into the charge continuity equation through the electrical conductivity σ which is a function of p, T, and Y_i. In the following section, a physical model for the current conservation will be illustrated along with two approaches to the solution of the Ampère's law: one based on the MVP and the other on the axisymmetric form of the BS law.

2.1. Physical modeling of the magnetostatics

By observing the governing equations above, it can be noted that there are only two equations for the three electromagnetic quantities $\boldsymbol{E}$, $\boldsymbol{j}$, $\boldsymbol{B}$ that appear in them. The missing equation is provided by the generalized Ohm's law [8], which in the "small Larmor radius" approximation, valid for plasma arcs in HVCBs, reads $\boldsymbol{j} = \sigma(\boldsymbol{E} + \boldsymbol{U} \times \boldsymbol{B})$. For HVCBs the $\boldsymbol{U} \times \boldsymbol{B}$ term is negligible with respect to the electric field, hence, in the following we will assume that $\boldsymbol{j} = \sigma \boldsymbol{E}$. The Gauss's law for magnetism $\nabla \cdot \boldsymbol{B} = 0$ is automatically fulfilled if the magnetic field is expressed as $\boldsymbol{B} = \nabla \times \boldsymbol{A}$, where $\boldsymbol{A}$ designates the MVP. Recalling the latter definition and introducing the electric scalar potential φ, it can be noted the Faraday's law of induction $\nabla \times \boldsymbol{E} = -\partial_t \boldsymbol{B}$ is satisfied by expressing the electric field as $\boldsymbol{E} = -\nabla\varphi - \partial_t \boldsymbol{A}$, which reduces to $\boldsymbol{E} = -\nabla\varphi$ under the present magnetostatic approximation.

2.1.1. Current conservation

In view of the relationships introduced above, equation (6) becomes

$$\nabla \cdot (\sigma \nabla \varphi) = 0. \tag{8}$$

The boundary conditions are $\partial_n \varphi = 0$ on all boundaries, apart from the ground contact where $\varphi = 0$ is imposed and the energized contact where $\varphi = c_1(t)$ is set. The factor c_1 is a function of time only and it is determined so that at each time it holds $\int_{S_\mathrm{c}} \sigma \nabla\varphi \cdot \boldsymbol{n} \, \mathrm{d}S = -I(t)$, where S_c is the surface of the energized contact through which the current $I(t)$ is flowing, while $\boldsymbol{n}$ is the unit vector normal to S_c pointing into the computational domain.

2.1.2. MVP formulation

In view of the assumptions discussed above, by using the Coulomb gauge $\nabla \cdot \boldsymbol{A} = 0$ and the vector identity $\nabla \times (\nabla \times \boldsymbol{A}) = \nabla(\nabla \cdot \boldsymbol{A}) - \nabla^2 \boldsymbol{A}$, equation (7) can be rewritten as

$$\nabla^2 \boldsymbol{A} = -\mu_0 \boldsymbol{j}. \tag{9}$$

The Poisson's equation (9) admits the solution

$$\boldsymbol{A}(\boldsymbol{r}) = \frac{\mu_0}{4\pi} \int_V \frac{\boldsymbol{j}(\boldsymbol{r}') \, \mathrm{d}V'}{|\boldsymbol{r} - \boldsymbol{r}'|} \tag{10}$$

which is computationally onerous for determining the MVP in each point of the domain V, but it can be

reasonably used for setting a Dirichlet boundary condition for equation (9). An approximated approach [9] for the boundary conditions takes advantage of the comparatively large size of HVCBs and the fact that $\boldsymbol{A}$ vanishes at infinity, as indicated by (10). In such approach, a zero flux boundary condition is imposed for the components of $\boldsymbol{A}$ on all outer edges of the computational domain, apart from one where the condition $\boldsymbol{A} = 0$ is imposed. It should be noted that having $\partial_n \boldsymbol{A} = 0$ on the entire frontier of the computational domain would be incompatible with equation (9), since it would lead to the impossible result $\int_V \boldsymbol{j}\,\mathrm{d}V = 0$, as can be readily verified by applying the divergence theorem to ∇A_x and ∇A_y. Such approximated formulation of the boundary conditions is the one we adopted in this work, as it can be straightforwardly implemented in ANSYS Fluent and, for HVCB applications, leads to an acceptable accuracy compared to that obtained by applying the exact boundary condition (10). It should be noted that no assumptions about symmetry have been made in the modeling of the MVP.

2.1.3. 2D–axi BS formulation

The assumption of rotational symmetry allows the arc and associated flow to be solved with a 2D–axi model. The computational domain for the latter is any of the planes passing through the axis of symmetry denoted as x axis. The y coordinate of this plane represents the radial distance from the x axis, see Figure 1.

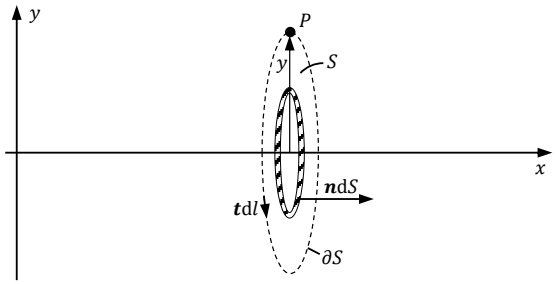

Figure 1. 2D–axi model. The directions of the unit vectors $\boldsymbol{t}$ *and* $\boldsymbol{n}$ *are linked by the right-hand rule.*

By taking the curl of (10) one obtains the BS law, which allows to compute the magnetic field knowing the current distribution that has generated it. Under the axisymmetry hypothesis, the magnetic field has only the azimuthal component and the BS law reduces to a simple expression. The latter can be readily derived with reference to Figure 1, by writing the Stokes' theorem for the vector $\boldsymbol{B}$ applied to the dashed circular loop of radius y, lying on a plane normal to the x axis:

$$\int_{\partial S} \boldsymbol{B}\cdot\boldsymbol{t}\,\mathrm{d}l = 2\pi y B(x,y) = \mu_0 \int_S \boldsymbol{j}\cdot\boldsymbol{n}\,\mathrm{d}S \qquad (11)$$

in which equation (7) has been used. The function $B(x,y)$ represents the azimuthal component of the magnetic field at the point P of axial coordinate x and radial coordinate y, while S is any surface having as boundary the dashed circumference passing through P. By choosing as a surface S, the circle bounded by said circumference, equation (11) can be expanded as $2\pi y B = \mu_0 \int_0^y j_x 2\pi y'\mathrm{d}y'$, which differentiated yields

$$\partial_y(yB) = \mu_0 y j_x. \qquad (12)$$

This equation expresses the BS formulation for 2D–axi models and it is solved with the boundary condition (11) on all the external edges of the computational domain. As can be seen, the axisymmetric BS formulation results in one equation less compared to the model based on the MVP. Moreover, the boundary condition (11) is much easier to implement than (10).

3. The numerical model

ANSYS Fluent offers the possibility of solving a generic transport equation for the scalar ϕ, called user defined scalar (UDS) equation [10], having the following form

$$\partial_t(\rho\phi) + \nabla\cdot(\boldsymbol{\psi}\phi) = \nabla\cdot(\Gamma\nabla\phi) + S_\phi. \qquad (13)$$

In this equation, the vector field $\boldsymbol{\psi}$ that appears in the advection term must be divergence free and it is, by default, set to $\boldsymbol{\psi} = \rho\boldsymbol{U}$. Two types of boundary conditions are permitted for the UDS equation: "specified value" and "specified flux". The former is a boundary condition of Dirichlet type that allows to set the value of the ϕ on the boundary. The latter is a special type of boundary condition that consists of setting the value of the flux $F_\phi = (-\boldsymbol{\psi}\phi + \Gamma\nabla\phi)\cdot\boldsymbol{n}$ on the boundary, where $\boldsymbol{n}$ is the unit normal vector pointing into the domain. In absence of convective term, this flux reduces to $F_\phi = \Gamma\partial_n\phi$ and the "specified flux" becomes a boundary condition of Neumann type.

3.1. Numerical models of the magnetostatics

The magnetostatic models described in Section 2.1 have been numerically implemented in ANSYS Fluent 2020 R2. The details of this implementation are provided below.

3.1.1. Current conservation implementation

The steady version of (13) with no advection nor source term is used for solving (8), by setting $\phi = \varphi$ and $\Gamma = \sigma$. The boundary conditions, as anticipated in Section 2.1, are specified value $\varphi = 0$ at the ground contact and specified value $\varphi = c_1(t)$ at the energized contact, where $c_1(t)$ is determined as described in Section 2.1. On all the other outer boundaries the specified flux boundary condition $F_\phi = 0$ is applied.

3.1.2. 2D–axi MVP implementation

The axial and radial projections of the vector equation (9) can be integrated with the 2D–axi solver of ANSYS Fluent, using the steady version of (13) without advection term. Specifically, the UDS equation for the axial projection of (9) is solved with $\phi = A_x$, $\Gamma = 1$, and

$S_\phi = \mu_0 j_x$, while the UDS equation for the radial projection is solved with $\phi = A_y$, $\Gamma = 1$, and $S_\phi = \mu_0 j_y$. As for the boundary conditions, in the numerical case presented below, they are for both equations: specified value $\varphi = 0$ on the farthest outer edge of the modeled geometry and specified flux $F_\phi = 0$ on all the other outer edges.

3.1.3. 2D–axi BS implementation

The BS law under the hypothesis of rotational symmetry yields equation (12) for computing the magnetic field. By dividing both sides of the latter by y, one gets an equation that can be solved with the 2D–axi solver of ANSYS Fluent, using the steady version of (13) without diffusion term. If $\boldsymbol{e}_y$ designates the unit vector along the y axis, it can be noted that choosing $\boldsymbol{\psi} = \boldsymbol{e}_y / y$ results in $\nabla \cdot \boldsymbol{\psi} = 0$, which is the requirement that the must be fulfilled by the UDS advection term. Moreover, recalling the expression of the nabla operator in cylindrical coordinates, the advection term can be expanded as $\nabla \cdot (\boldsymbol{\psi}\phi) = \boldsymbol{\psi} \cdot \nabla\phi = (1/y)\,\partial_y \phi$. The setup of the UDS formulation of (12) is then completed by letting $\phi = yB$ and $S_\phi = \mu_0 j_x$. The boundary condition is of specified value type and it is expressed by (11) on all the outer edges of the domain.

3.2. Results of a validation case

Simulations have been performed to reproduce the pressure as a function of time measured in an experiment conducted at our High-Voltage Laboratory. In the test, operated in ambient air, an arc is ignited by exploding wire inside the cylindrical throat of a PTFE tube, between two plug electrodes. Due to the strong evaporation the arc burns in a gaseous mixture composed almost entirely of PTFE vapor. The experimental mockup exhibits rotational symmetry and its cross-section with a plane passing through the axis of symmetry is depicted in Figure 2 along with the main dimensions. The pressure is measured at the point S_1 located in the middle of the tube throat.

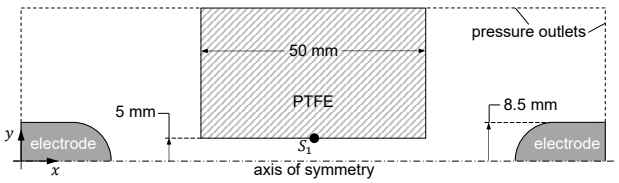

Figure 2. 2D–axi computational domain.

The figure also illustrates the extent of the computational domain for the 2D–axi simulations. At the pressure outlets the ambient pressure is prescribed. The computational grid was predominantly structured. For the simulation with the BS model only the the fluid domain was meshed, while in the case of the MVP model the electrodes and polymeric tube were also meshed. The spatial resolution and the time stepping were selected in order to ensure a properly converged solution. Figure 3 shows the pressure distribution obtained with the arc simulation tool featuring the BS formulation detailed above. The contour plot refers to the time when the current attains its peak value.

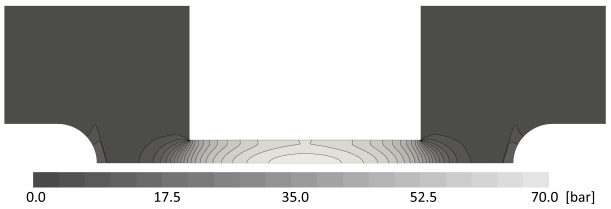

Figure 3. Pressure distribution at current peak for the 2D–axi BS implementation.

In Figure 4 the pressures at the sensor location simulated with both BS and VP models are reported along with the measured pressure and the current used in the arcing operation. As can be seen, both methods for computing the magnetic field yield almost the same pressure, with a relative difference smaller than 1%. Moreover, the simulated pressures exhibit a good agreement with the measured one.

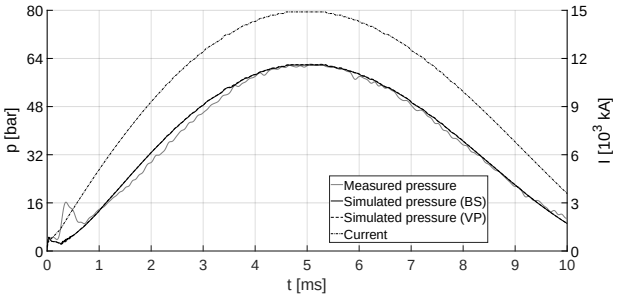

Figure 4. Simulated vs. measured pressures at S_1.

As for the importance of magnetic effects for this validation case, at current peak the pressure computed without magnetic field at S_1 is 11.6% higher than that obtained when Lorentz forces are included.

4. Conclusions

This work deals with the modeling of the magnetic field in an arc simulation tool based on a commercial flow solver (ANSYS Fluent). It is shown that the differential form of the axisymmetric Biot-Savart law is suited to be represented by the generic transport equation available in the commercial software, while its integral form provides the corresponding boundary condition. The arc simulation tool is applied to reproduce numerically the pressure measured in an experiment in which a rotationally symmetric plasma arc was established. The numerical reproductions are performed with a two–dimensional axisymmetric flow solver, using both the Biot-Savart model and the Ampère's law formulated in terms of magnetic vector potential. The former model despite being less computationally expensive yields a simulated pressure nearly identical to that of the latter model and in good agreement with the measured signal.

References

[1] P. Freton, J. J. Gonzalez, M. Masquère, and F. Reichert. Magnetic field approaches in dc thermal plasma modelling. *Journal of Physics D: Applied Physics*, 44(34):345202, aug 2011. doi:10.1088/0022-3727/44/34/345202.

[2] C. B. Ruchti and L. Niemeyer. Ablation controlled arcs. *IEEE Transactions on Plasma Science*, 14(4):423–434, 1986. doi:10.1109/TPS.1986.4316570.

[3] J. Tepper, M. Seeger, T. Votteler, et al. Investigation on erosion of cu/w contacts in high-voltage circuit breakers. *IEEE Transactions on Components and Packaging Technologies*, 29(3):658–665, 2006. doi:10.1109/TCAPT.2006.880476.

[4] C. Doiron and K. Hencken. Calculation of thermodynamic and transport properties of thermal plasmas based on the cantera software toolkit. *APS Meeting Abstracts*, 3:3001, 2013. URL: http://meetings.aps.org/link/BAPS.2013.GEC.TF3.1.

[5] Kurucz database. http://kurucz.harvard.edu/.

[6] TopBase database. http://cdsweb.u-strasbg.fr/topbase/topbase.html.

[7] B. Galletti, F. Kassubek, M. Buffoni, et al. Numerical investigation, including experimental validation, of an axially blown, stable arc in argon. *Plasma Physics and Technology*, 6(1):78–81, July 2019.

[8] R. J. Goldston and P. H. Rutherford. *Introduction to Plasma Physics (First Edition)*. CRC Press, 1995. ISBN 9780750301831.

[9] P. Freton, J. J. Gonzalez, and A. Gleizes. Comparison between a two- and a three-dimensional arc plasma configuration. *Journal of Physics D: Applied Physics*, 33(19):2442–2452, oct 2000. doi:10.1088/0022-3727/33/19/315.

[10] Ansys® Fluent, Release 2020 R2. *ANSYS Fluent Customization Manual*. ANSYS, Inc., 2020.